

# SCIENTIFIC REPORTS



OPEN

## Europium (III) Organic Complexes in Porous Boron Nitride Microfibers: Efficient Hybrid Luminescent Material

Jing Lin<sup>1,2</sup>, Congcong Feng<sup>1,2</sup>, Xin He<sup>1,2</sup>, Weijia Wang<sup>1,2</sup>, Yi Fang<sup>1,2</sup>, Zhenya Liu<sup>1,2</sup>, Jie Li<sup>1,2</sup>, Chengchun Tang<sup>1,2</sup> & Yang Huang<sup>1,2</sup>

Received: 18 July 2016  
Accepted: 15 September 2016  
Published: 30 September 2016

We report the design and synthesis of a novel kind of organic-inorganic hybrid material via the incorporation of europium (III)  $\beta$ -diketonate complexes ( $\text{Eu}(\text{TTA})_3$ , TTA = 2-thenoyltrifluoroacetone) into one-dimensional (1D) porous boron nitride (BN) microfibers. The developed  $\text{Eu}(\text{TTA})_3@$ BN hybrid composites with typical 1D fibrous morphology exhibit bright visible red-light emission on UV illumination. The confinement of  $\text{Eu}(\text{TTA})_3$  within pores of BN microfibers not only decreases the aggregation-caused quenching in solid  $\text{Eu}(\text{TTA})_3$ , but also improves their thermal stabilities. Moreover, The strong interactions between  $\text{Eu}(\text{TTA})_3$  and porous BN matrix result in an interesting energy transfer process from BN host to TTA ligand and TTA ligand to  $\text{Eu}^{3+}$  ions, leading to the remarkable increase of red emission. The synthetic approach should be a very promising strategy which can be easily expanded to other hybrid luminescent materials based on porous BN.

Researches on organic-inorganic hybrid materials have gathered immense attention because of their potential applications in various fields such as sensing, light-emitting, lithium ion battery, etc<sup>1-5</sup>. The combination of organic and inorganic components at a nanometer scale could allow us to generate unique properties in such complex systems. For example, encapsulating organic dyes into porous metal-organic frameworks (MOFs) can efficiently enhance their fluorescence quantum efficiency and tuning the emission color due to the confinement of dyes in the pores of MOFs<sup>2</sup>.

Trivalent lanthanide complexes with organic ligands are of great interest due to their outstanding luminescent properties. On one hand, lanthanide complexes could possess of characteristic and narrow emission bands with a full width at half maximum of less than 10 nm and long-lived excited states gaining from the luminescent centres of trivalent lanthanide ions ( $\text{Ln}^{3+}$ ). On the other hand, differing from the  $\text{Ln}^{3+}$  ions which have poor light absorption abilities due to the forbidden intraconfiguration  $f-f$  transition, lanthanide complexes exhibit sensitized emission because the organic ligands have large molar absorption coefficients and can effectively increase light absorption by “antenna effect”<sup>6,7</sup>. In spite of the outstanding luminescent properties of lanthanide complexes, the practical application of these complexes has still been limited due to their poor thermal stability and processibility<sup>8</sup>. To solve this problem, introducing lanthanide complexes in a stable porous matrix to form organic-inorganic hybrid materials has been intensively studied. So far, inorganic porous materials, such as zeolites<sup>9-11</sup>, mesoporous silica (SBA-15, MCM-41, etc)<sup>12-18</sup> have been used as the matrix due to their special porous structure and thermal and chemical stabilities. The confinement of lanthanide complexes within porous matrix can not only improve their stabilities, but also decrease the aggregation-caused quenching in lanthanide complex, which would be beneficial for the effective luminescence<sup>19</sup>.

Porous boron nitride (BN) has attractive properties including low density, high thermal conductivity, superior oxidation resistance and chemical inertness. Particularly, the recently breakthrough on the preparation of porous BN with high specific surface areas and large pore volumes has gained this porous material much attention<sup>20-28</sup>. We envision that porous BN can be an ideal candidate as the matrix for lanthanide complexes. Notwithstanding

<sup>1</sup>School of Materials Science and Engineering, Hebei University of Technology, Tianjin, 300130, P. R. China. <sup>2</sup>Hebei Key Laboratory of Boron Nitride Micro and Nano Materials, Hebei University of Technology, Tianjin, 300130, P. R. China. Correspondence and requests for materials should be addressed to J.L. (email: linjing@hebut.edu.cn) or Y.H. (email: huangyang@hebut.edu.cn)

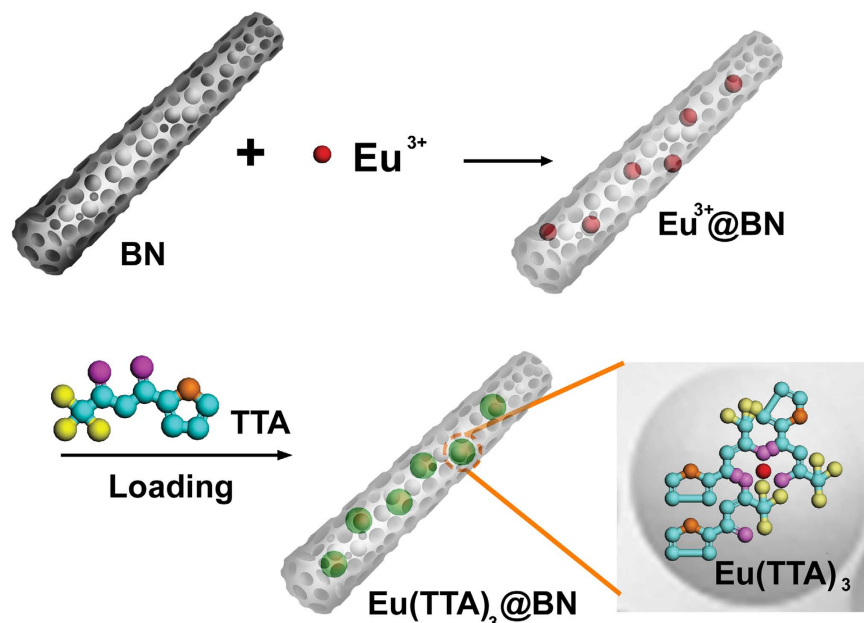


**Figure 1.** Illustration of the procedure for synthesis of  $\text{Eu}(\text{TTA})_3@ \text{BN}$  hybrid microfibers.

the possibility, porous BN holding characteristic  $\text{sp}^2$ -bonded honeycomb structure is quite different with the traditional oxide porous matrix from both the chemical and physical view of point. So-derived specific interactions with the lanthanide complexes will surely influence the luminescence performance of the constructed hybrid materials. Unfortunately, such lanthanide complex/porous BN hybrid luminescent materials have not been explored so far.

In this paper, we report the design of novel lanthanide complex/porous BN organic-inorganic hybrid materials via the incorporation of europium (III)  $\beta$ -diketonate complexes ( $\text{Eu}(\text{TTA})_3$ , TTA = 2-thenoyltrifluoroacetone) into porous BN microfibers. The  $\text{Eu}(\text{TTA})_3@ \text{BN}$  composite possesses one-dimensional (1D) fibrous morphology similar with pure porous BN matrix. The emission intensity and lifetime of  $\text{Eu}^{3+}$  ions are significantly enhanced compared with pure europium complexes. The thermal stability of  $\text{Eu}(\text{TTA})_3$  has also been improved due to the protection of porous BN matrix. Interestingly, due to the strong interactions between europium complexes and porous BN, efficient energy transfer from BN to TTA ligand and TTA ligand to  $\text{Eu}^{3+}$  ions takes place in the hybrid system, leading to the great enhancement of red emission. This novel organic-inorganic hybrid material is envisaged to become highly valuable in lighting devices and biomedical analysis.

## Results and Discussion

Figure 1 illustrates the procedure for synthesis of the organic-inorganic hybrid material  $\text{Eu}(\text{TTA})_3@ \text{BN}$ . The porous BN products used as the inorganic hosts are mainly some microfibers with main characteristic pore sizes of  $\sim 1.3$  and  $\sim 3.9$  nm. The specific surface area of the porous BN is  $\sim 1600 \text{ m}^2 \text{ g}^{-1}$  and the pore volume is  $\sim 0.9 \text{ cm}^3 \text{ g}^{-1}$ <sup>23</sup>. The synthesis of  $\text{Eu}(\text{TTA})_3@ \text{BN}$  was realized via a two-step method: the loading of  $\text{Eu}^{3+}$  ions into porous BN microfibers was achieved by adsorption of  $\text{Eu}^{3+}$  ions in ethanol solution dispersed with porous BN, and then the organic ligands TTA was inserted into  $\text{Eu}^{3+}@ \text{BN}$  by a gas diffusion method. Our previous studies indicate that the as-prepared porous BN exhibits excellent adsorption performance for various metal ions due to their high specific area, large pore volume and dipolar nature of B-N bonds. Especially, the surface of porous BN is negatively charged, so the metal ions can be adsorbed on porous BN by the electrostatic interactions<sup>23,24</sup>. After obtaining  $\text{Eu}^{3+}@ \text{BN}$  microfibers, the formation of organic-inorganic hybrid  $\text{Eu}(\text{TTA})_3@ \text{BN}$  can be realized by coordination reaction between TTA and  $\text{Eu}^{3+}$  ions in porous BN microfibers. X-ray diffraction (XRD) result of hybrid product is quite similar to that of starting porous BN, indicating the amorphous phase of organic  $\text{Eu}(\text{TTA})_3$  (Supporting Information, Fig. S1).

The microstructures and compositions of the  $\text{Eu}(\text{TTA})_3@ \text{BN}$  hybrid product were further examined in transmission electron microscopy (TEM). A typical low-magnification TEM image (Fig. 2a) indicates that the product keeps fibrous morphology as as-prepared porous BN microfiber. The diameter of the microfiber here is  $\sim 0.5 \mu\text{m}$ . The bright spots on the microfiber shown in the enlarged TEM image (Fig. 2b) reveal some mesopores with the diameters of tens nm existing in the microfiber. Figure 2b also shows that the surface of the microfiber is quite clear. High resolution TEM image in Fig. 2c shows the edge of the microfiber. The crystallized BN layers (marked by the arrows) is very clear without any adhered substances. High resolution TEM image (Fig. 2d) taking from the centre of the microfibers shows an amorphous phase covered over the microfiber. The amorphous phase could be attributed to the  $\text{Eu}(\text{TTA})_3$  on BN microfibers. To further confirm our success in introducing  $\text{Eu}(\text{TTA})_3$ , a composition analysis was carried out. Figure 2e,f show scanning transmission electron microscopy (STEM) image and the corresponding energy-dispersive X-ray spectroscopy (EDS) spectrum taken from a single  $\text{Eu}(\text{TTA})_3$

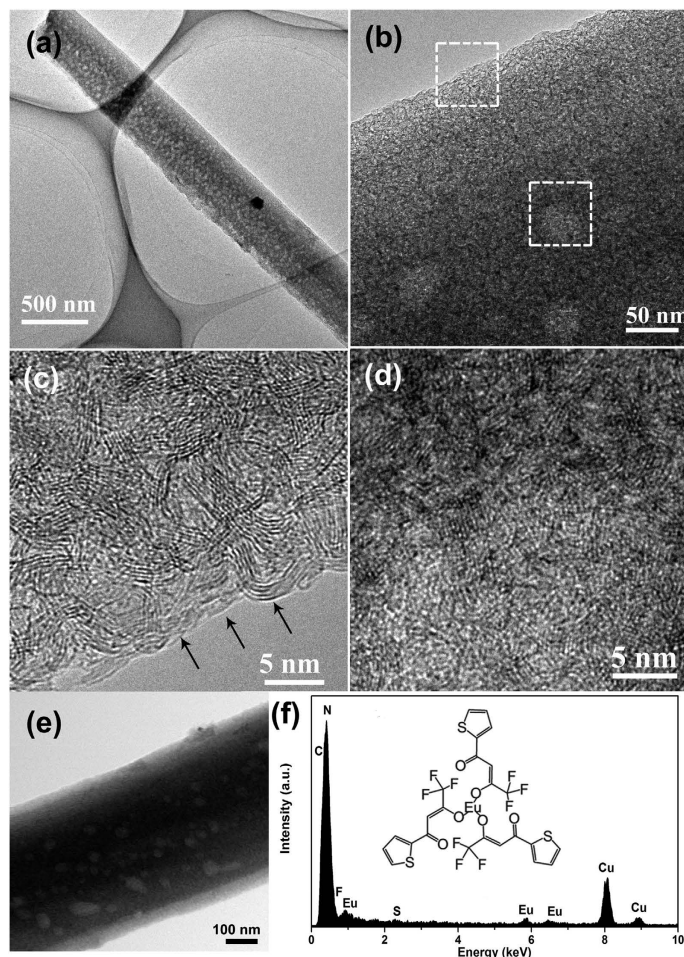


**Figure 2.** (a) Low-magnification TEM image of  $\text{Eu}(\text{TTA})_3@ \text{BN}$  hybrid product, revealing the fibrous morphology; (b) Enlarged TEM image of the microfiber; (c, d) HRTEM images taken from the two areas labelled by the two dashed frames marked in (b), respectively; (e) STEM image and (f) the corresponding EDS spectrum taken from a single  $\text{Eu}(\text{TTA})_3@ \text{BN}$  microfiber.

@BN microfiber. The peaks from C, F, Eu and S elements can be seen clearly. So we can confirm that the organic lanthanide complexes,  $\text{Eu}(\text{TTA})_3$ , have been successfully introduced into the BN microfibers. Besides, the specific surface area of  $\text{Eu}(\text{TTA})_3@ \text{BN}$  microfibers has been measured as low as  $\sim 70 \text{ m}^2 \text{ g}^{-1}$ . Compared with pure porous BN microfibers which possess a very high specific surface area ( $\sim 1600 \text{ m}^2 \text{ g}^{-1}$ ), the significantly decrease of specific surface area implies that the lanthanide complexes have been encapsulated inside the pores of the BN. With a brief summary of the above results, we infer that the lanthanide complexes could be encapsulated inside the pore channels of BN microfiber, rather than coated on their outside surface.

Fourier transform infrared (FTIR) analysis was utilized to study the loading of  $\text{Eu}(\text{TTA})_3$  in porous BN. Figure 3 shows the FTIR spectrum of as-prepared  $\text{Eu}(\text{TTA})_3@ \text{BN}$  sample. The spectra of pure porous BN and  $\text{Eu}^{3+}@ \text{BN}$  are also shown for comparison. The FTIR spectrum of porous BN shows peaks at  $\sim 1391 \text{ cm}^{-1}$  and  $\sim 805 \text{ cm}^{-1}$ , corresponding to B-N stretching vibrations and B-N-B bending vibrations<sup>29</sup>, respectively. The peak at  $\sim 3426 \text{ cm}^{-1}$  is attributed to the vibrations of B-OH/B-NH<sub>2</sub> group<sup>23</sup>. In comparison, the FTIR spectrum of  $\text{Eu}^{3+}@ \text{BN}$  is quite similar to that of porous BN, although XPS analysis (Fig. S2, Supporting Information) clearly indicates that the  $\text{Eu}^{3+}$  has already been loaded. There is no noticeable shift for all the peaks from porous BN after incorporating of  $\text{Eu}^{3+}$ , which means that the  $\text{Eu}^{3+}$  ions are adsorbed on BN by weak interactions, i.e. electrostatic interactions, rather than strong chemical bonding. After loading of  $\text{Eu}^{3+}$  and TTA on the porous BN successively, some new absorption peaks at  $\sim 1617 \text{ cm}^{-1}$ ,  $\sim 1093 \text{ cm}^{-1}$  and  $\sim 468 \text{ cm}^{-1}$  can be observed. The peak at  $\sim 1617 \text{ cm}^{-1}$  is assigned to the C=O stretching band which is related to the ligand (TTA); the peak at  $\sim 468 \text{ cm}^{-1}$  could be attributed to the stretching Eu-O bond, indicating ligands are indeed coordinated with  $\text{Eu}^{3+}$  ions through the oxygen in the complex ligands; another peak observed at  $\sim 1093 \text{ cm}^{-1}$  is corresponds to the B-N-O group, indicating that the strong interactions also occur between ligand TTA and BN host. The strong interaction between the europium complexes and porous BN is very important for avoiding the nonhomogeneous distribution and leakage of lanthanide complexes in the porous matrix.

The excitation and emission spectra of  $\text{Eu}(\text{TTA})_3@ \text{BN}$  microfibers were examined at room temperature. The excitation spectrum monitored at 615 nm displays a broad band ranging from 250 to 400 nm (Fig. 4a). The absence of sharp peaks corresponding to the  $f-f$  transitions of  $\text{Eu}^{3+}$  ions indicates that effective energy transfer

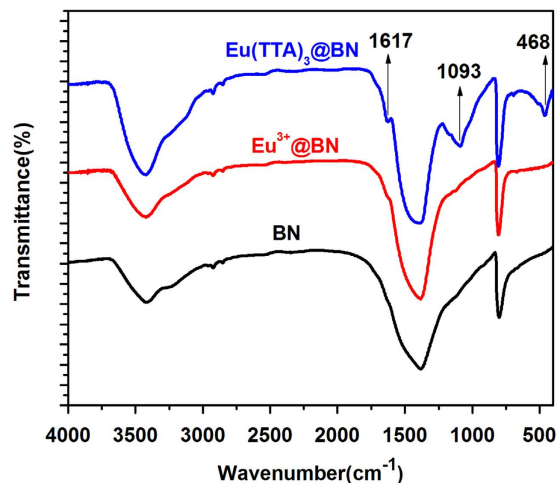


**Figure 3.** FTIR spectra of porous BN (a),  $\text{Eu}^{3+}$ @BN (b) and  $\text{Eu}(\text{TTA})_3$ @BN (c) samples.

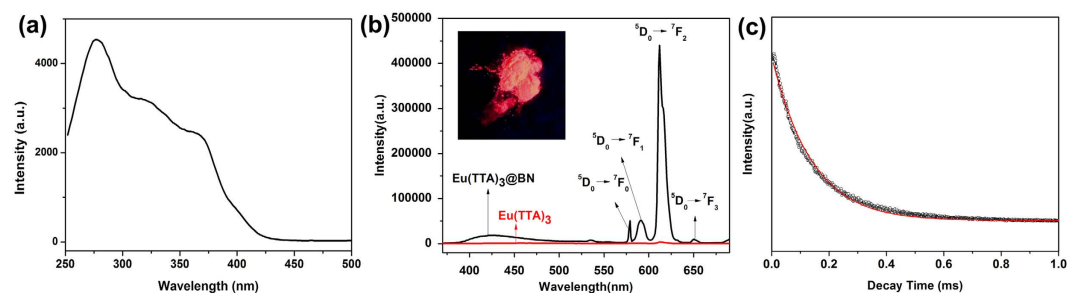


**Figure 4.** (a) Excitation spectrum of  $\text{Eu}(\text{TTA})_3$ @BN samples monitored at 615 nm. (b) Emission spectra of  $\text{Eu}(\text{TTA})_3$ @BN and solid  $\text{Eu}(\text{TTA})_3 \cdot n\text{H}_2\text{O}$  samples excited by 280 nm. (inset) Photo image of  $\text{Eu}(\text{TTA})_3$ @BN excited by UV light, showing intense red light emission. (c) Decay curve of  $\text{Eu}(\text{TTA})_3$ @BN sample.

takes place to  $\text{Eu}^{3+}$  ions<sup>8</sup>. Upon excited at 280 nm, the  $\text{Eu}(\text{TTA})_3$ @BN exhibits intense red emission with characteristic peaks of 581, 591, 615 and 653 nm, which correspond to the excited state  ${}^5\text{D}_0 \rightarrow {}^7\text{F}_J$  ( $J = 0-3$ ) of  $\text{Eu}^{3+}$  ions, respectively (Fig. 4b). To make comparisons, we also measured the emission spectrum of pure  $\text{Eu}(\text{TTA})_3 \cdot n\text{H}_2\text{O}$  in the solid state. As shown in Fig. 4b, very weak emission can be observed in solid  $\text{Eu}(\text{TTA})_3 \cdot n\text{H}_2\text{O}$ . The results demonstrate that after loading of  $\text{Eu}(\text{TTA})_3$  in BN host, the nonradiative energy transfer process between  $\text{Eu}(\text{TTA})_3$  can be successfully restrained, which would otherwise quench the red emission. The intense red light emission can be easily visible by eye upon 365 nm UV excitation, as shown in inset of Fig. 4b. The decay curve of  $\text{Eu}(\text{TTA})_3$ @BN under excitation of 280 nm is shown in Fig. 4c. The curve can be well fitted mono-exponentially and the value of lifetime  $\tau$  is calculated to be 0.361 ms. This value is longer than lifetime of pure  $\text{Eu}(\text{TTA})_3 \cdot n\text{H}_2\text{O}$  ( $\tau = 0.21$  ms, shown in Supporting Information, Fig. S3), which can be attributed to the inhibition of nonradiative deactivation pathways by confinement in the pores of BN host<sup>8</sup>.

In order to further clarify the reason for the great enhancement of red emission in the  $\text{Eu}(\text{TTA})_3$ @BN system, we compare the photoluminescence (PL) of pure BN,  $\text{Eu}^{3+}$ @BN and  $\text{Eu}(\text{TTA})_3$ @BN samples, as shown in Fig. 5a. Pure porous BN microfibers exhibit strong UV emission centered at  $\sim 320$  nm, which can be attributed to the defect-related centers or intrinsic impurities in BN<sup>30</sup>. After adsorption of  $\text{Eu}^{3+}$ , the  $\text{Eu}^{3+}$ @BN sample shows similar UV emission band and a very weak peak at  $\sim 613$  nm, which corresponds to the red emission of  $\text{Eu}^{3+}$  ions. Since the  $f-f$  transitions of lanthanide ions are spin forbidden, it is hard to generate efficient luminescence emission by direct excitation. Through coordination to TTA ligands, the red emission intensity of  $\text{Eu}(\text{TTA})_3$ @BN is significantly enhanced, which can be attributed to the “antenna effect”<sup>31,32</sup>. Effective energy transfer from TTA ligands to  $\text{Eu}^{3+}$  ions takes place, resulting in sensitized red emission. Interestingly, we also find the UV emission of BN host disappears in  $\text{Eu}(\text{TTA})_3$ @BN, and a weak broad band centered at  $\sim 450$  nm can be obtained. The  $\sim 450$  nm band origins from the C- and/or O-related impurities in BN<sup>33,34</sup>. After coordination of TTA ligands with  $\text{Eu}^{3+}$  ions in BN host, the formation of B-N-O bonds makes it possible to obtain the weak blue emission from BN. Besides, the great suppressed UV emission indicates effective energy transfer from BN host to  $\text{Eu}(\text{TTA})_3$  may be occurred. As shown in Fig. 5b, the absorption spectrum of TTA shows a broad band between 200 and 450 nm, while the pure BN host exhibits strong UV emission centered at  $\sim 320$  nm. The spectral overlap between the emission of BN host and absorption of TTA results in an efficient BN-to-TTA energy transfer behavior. PL maps of BN host and  $\text{Eu}(\text{TTA})_3$  also indicate similar energy transfer results (Supporting Information, Fig. S4). We believe the energy transfer process in the  $\text{Eu}(\text{TTA})_3$ @BN system can be described as follows (Fig. 5c)<sup>6</sup>: (1) the BN host is excited from the ground state to the excited state by absorbing UV energy; (2) the energy of the BN

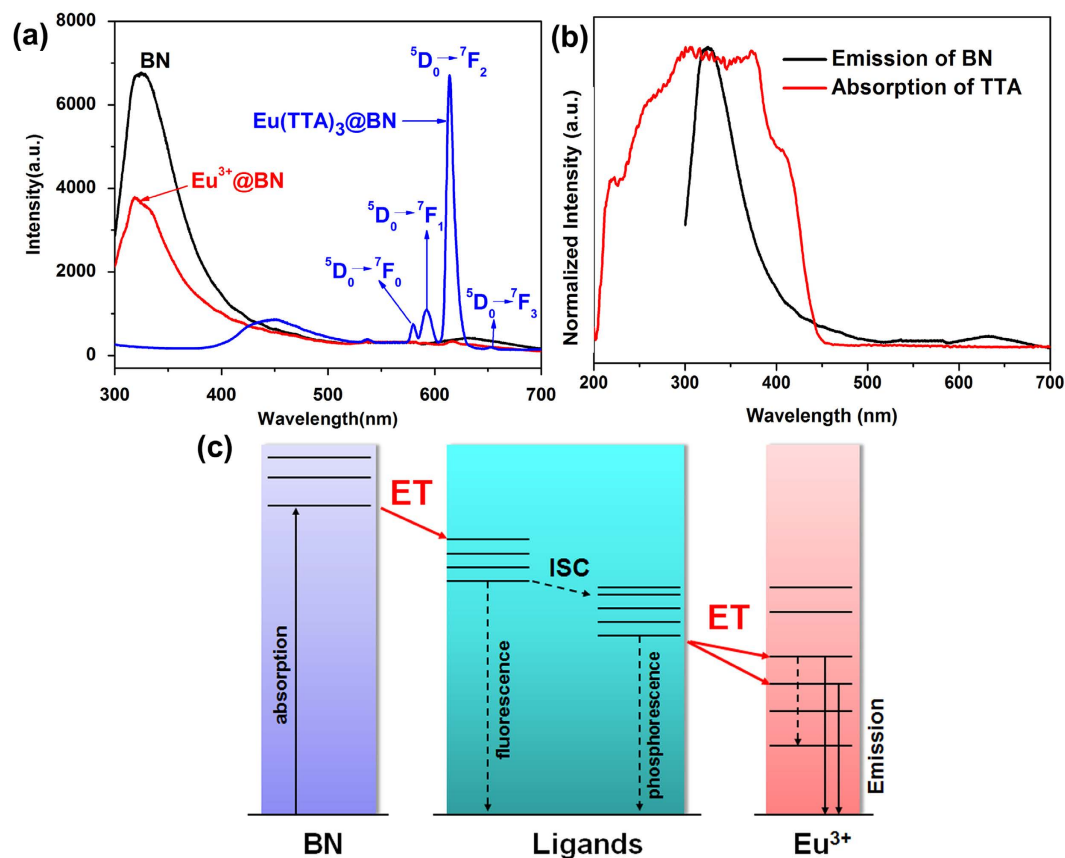


**Figure 5.** (a) Emission spectra of pure BN (black),  $\text{Eu}^{3+}@BN$  (red) and  $\text{Eu}(\text{TTA})_3@BN$  (blue) samples. (b) Emission spectrum of pure BN (black) and UV-vis absorption spectrum of ligands TTA (red). (c) The schematic of the energy transfer process in  $\text{Eu}(\text{TTA})_3@BN$  system. ET = energy transfer, ISC = intersystem crossing.

excited state is transferred to the ligands TTA; (3) the ligands TTA is excited to the singlet excited state, and then the energy is transferred to the triplet excited state through intersystem crossing (ISC); (4) energy transfers from the triplet state of the ligands to the excited  $4f$  states of  $\text{Eu}^{3+}$  ions; (5) red emission can be obtained through the  $f-f$  transitions in  $\text{Eu}^{3+}$  ions. This interesting energy transfer process is quite different from those in earlier reported hybrid system, i.e. lanthanide complexes encapsulated in zeolites, SBA-15, MCM-41, etc, in which only effective energy transfer from the organic ligands to the  $\text{Ln}^{3+}$  ion (the so-called “antenna effects”) takes place. Herein our results represent that when the  $\text{Eu}(\text{TTA})_3@BN$  hybrid system is excited at 280 nm, efficient energy transfer of BN-to-TTA-to- $\text{Eu}^{3+}$  occurs, leading to the great enhancement of red emission.

We have also studied the PL properties of  $\text{Eu}(\text{TTA})_3@BN$  samples with different weak broad blue band emission and intense red emission peaks. With an increase of Eu contents from 0.00005 mol/L to 0.005 mol/L, the intensity of blue band decreases gradually, while the intensity of red emission peaks increases significantly. However, when the Eu contents increases to 0.05 mol/L, a great decrease of red emission has been observed. The PL quenching may result from the nonradiative energy transfer process between  $\text{Eu}(\text{TTA})_3$  in a high concentration.

The thermal stability of  $\text{Eu}(\text{TTA})_3@BN$  sample was studied by thermogravimetric (TG) analysis in the presence of air. Besides, the thermal stability of pure  $\text{Eu}(\text{TTA})_3 \cdot n\text{H}_2\text{O}$  was also studied for comparison. As shown in Fig. 6a, the curve of pure  $\text{Eu}(\text{TTA})_3 \cdot n\text{H}_2\text{O}$  complex shows a weight loss of ~54% for the entire process. The first weight loss peak at 195 °C corresponds to the loss of coordinate water, indicating the decomposition of the complexes starts. The weight loss occurs between 230 °C and 550 °C can be attribute to the decomposition of  $\text{Eu}(\text{TTA})_3$ . In detail, the second peak at 293 °C is related to the decomposition of the three ligands in the complex, while the third peak appears at 507 °C is due to the oxidation of the complex and finally  $\text{Eu}_2\text{O}_3$  could be generated<sup>35</sup>. Figure 6b shows the TG curve of  $\text{Eu}(\text{TTA})_3@BN$ , displaying a weight loss of only ~7.8% for the entire process. The first fast weight loss step starts from room temperature and ends at about 50 °C, with a weight loss of ~2%, is related to the remaining gas desorption from the sample. The second step shows a weight loss peak at 355 °C due to the decomposition of  $\text{Eu}(\text{TTA})_3$ . The comparison indicates that the  $\text{Eu}(\text{TTA})_3@BN$  hybrid material displays greatly enhanced thermal stability compared to the pure  $\text{Eu}(\text{TTA})_3 \cdot n\text{H}_2\text{O}$  complex. We believe that the space restriction of the europium (III) complexes by the pores of BN microfibers is the main factor for the improvement of their thermal stability.

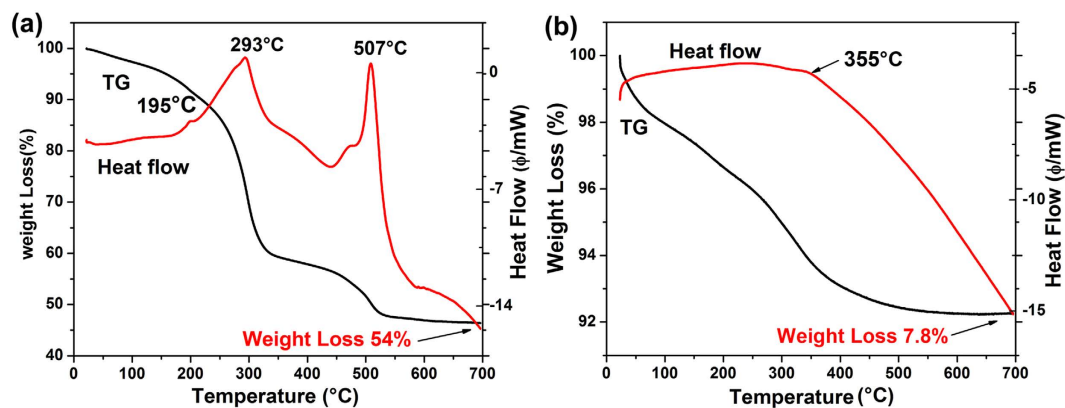


**Figure 6.** TG-DTA curves of (a)  $\text{Eu}(\text{TTA})_3 \cdot n\text{H}_2\text{O}$  and (b)  $\text{Eu}(\text{TTA})_3 @ \text{BN}$ , in the presence of air.

## Conclusions

We designed and synthesized a novel kind of organic-inorganic hybrid materials via the incorporation of europium (III) complexes into 1D porous BN microfibers. TEM analysis demonstrated the amorphous europium (III) complexes were encapsulated inside porous BN, forming 1D  $\text{Eu}(\text{TTA})_3 @ \text{BN}$  hybrid composites. The developed  $\text{Eu}(\text{TTA})_3 @ \text{BN}$  hybrid composites showed bright visible red-light emission on UV illumination. Our results demonstrated an interesting and efficient energy transfer from BN host to TTA ligand and TTA ligand to  $\text{Eu}^{3+}$  ions occurred during the photoluminescence process, which was quite different from earlier reports regarding lanthanide complexes encapsulated within other porous matrix. The confinement of the europium (III) complexes within the pores of BN microfibers not only improved their thermal stabilities, but also decreased the aggregation-caused quenching in solid europium (III) complexes, leading to the remarkable increase of red emission. The designed synthetic approach we report here offers a great flexibility in rational design of many other hybrid luminescent materials based on porous BN.

## Experimental Section

**Starting materials.** Porous BN microfibers were synthesized in relation to the reported procedure using  $\text{H}_3\text{BO}_3$  and  $\text{C}_3\text{N}_6\text{H}_6$  as the starting materials<sup>23</sup>. 2-Thenoyltrifluoroacetone (99%, TTA, Aldrich) was used as standard.  $\text{Eu}(\text{TTA})_3 \cdot n\text{H}_2\text{O}$  was produced by the reported method<sup>35</sup>. All the other reagents are analytical pure.

**Preparation of  $\text{Eu}^{3+} @ \text{BN}$  microfibers.** Firstly, loading of  $\text{Eu}^{3+}$  ions into porous BN microfibers was achieved by adsorption method. Briefly, 1 g of porous BN microfibers were dispersed in 1 L of ethanol to obtain a BN suspension. Then  $\text{Eu}(\text{NO}_3)_3 \cdot 6\text{H}_2\text{O}$  was dissolved in ethanol with a desired concentration (0.0005 mol/L), and added dropwise into the BN suspension. Then the mixed solution was stirred for 12 h and filtered. After drying at 80 °C in air overnight, white powder was obtained.

**Synthesis of  $\text{Eu}(\text{TTA})_3 @ \text{BN}$  microfibers.**  $\text{Eu}(\text{TTA})_3 @ \text{BN}$  microfibers were prepared by a gas diffusion method. In detail, 0.42 g of the as-prepared  $\text{Eu}^{3+} @ \text{BN}$  white powder and 0.33 g of TTA were grinded together and then put into a gas diffusion flask. The flask was set inside of oil bath pan at 60 °C for 1 h under a vacuum condition. Then the temperature was raised up to 100 °C and kept for 24 h. Finally, the products were washed with acetonitrile and dried in air at 80 °C, respectively.

**Characterization.** The structures of the as-prepared samples were characterized using an X-ray powder diffraction (XRD, BRUKER D8 FOCUS). The chemical bonding state of the products and the surface functional groups was examined by a Fourier transform infrared spectrophotometer (FTIR) (VECTOR22). The microstructures and compositions of the products were analysed using a transmission electron microscope (TEM, Philips Tecnai F20) equipped with an energy-dispersive X-ray spectrometer (EDS). For this, the powder samples were dispersed in ethanol, and then dripped dropwise onto the copper meshes covered with holey carbon films. The luminescent properties of the products were measured on the fluorescence spectrophotometer (F-7000 and FL3-22) and thermal stability analysis was carried out using a thermogravimetric analyzer (TG) (SDT Q-600) under normal atmosphere with stream of (100 mL  $\text{min}^{-1}$ ), at a heating rate of 5 °C  $\text{min}^{-1}$ .

## References

- Dong, M. J., Zhao, M., Ou, S., Zou, C. & Wu, C. D. A luminescent dye @MOF platform: emission fingerprint relationships of volatile organic molecules. *Angew. Chem. Int. Ed.* **53**, 1575–1579 (2014).
- Cui, Y. J. *et al.* Dye encapsulated metal-organic framework for warm-white LED with high color-rendering index. *Adv. Funct. Mater.* **25**, 4796–4802 (2015).
- Suresh, V. M., George, S. J. & Maji, T. K. MOF nano-vesicles and toroids: self-assembled porous soft-hybrids for light harvesting. *Adv. Funct. Mater.* **23**, 5585–5590 (2013).
- Zhang, J. F. *et al.* Solid polymer electrolyte membranes based on organic/inorganic nanocomposites with star-shaped structure for high performance lithium ion battery. *J. Membrane Sci.* **509**, 138–148 (2016).
- Gao, Q. S., Chen, P., Zhang, Y. H. & Tang, Y. Synthesis and characterization of organic-inorganic hybrid  $\text{GeOx}/\text{Ethylene diamine}$  nanowires. *Adv. Mater.* **20**, 1837–1842 (2008).

6. Feng, J. & Zhang, H. J. Hybrid materials based on lanthanide organic complexes: a review. *Chem. Soc. Rev.* **42**, 387–410 (2013).
7. Yan, B. Recent progress in photofunctional lanthanide hybrid materials. *RSC Advances*. **2**, 9304–9324 (2012).
8. Binnemans, K. Lanthanide-Based Luminescent Hybrid Materials. *Chem. Rev.* **109**, 4283–4374 (2009).
9. Li, P., Wang, Y. G., Li, H. R. & Calzaferri, G. Luminescence enhancement after adding stoppers to europium (III) nanozeolite L. *Angew. Chem. Int. Ed.* **53**, 2904–2909 (2014).
10. Li, H. R., Li, M., Wang, Y. & Zhang, W. J. Luminescent hybrid materials based on laponite clay. *Chem. Eur. J.* **20**, 10392–10396 (2014).
11. Wang, T. R., Li, P. & Li, H. R. Color-tunable luminescence of organoclay-based hybrid materials showing potential applications in white LED and thermosensors. *ACS Appl. Mater. Interfaces*. **6**, 12915–12921 (2014).
12. Yan, B. & Zhou, B. Two photoactive lanthanide (Eu<sup>3+</sup>, Tb<sup>3+</sup>) hybrid materials of modified  $\beta$ -diketone bridge directly covalently bonded mesoporous host (MCM-41). *J. Photochem. Photobiol. A*. **195**, 314–322 (2008).
13. Li, Y. & Yan, B. Lanthanide (Tb<sup>3+</sup>, Eu<sup>3+</sup>) functionalized MCM-41 through modified *Meta*-aminobenzoic acid linkage: covalently bonding assembly, physical characterization and photoluminescence. *Micropor. Mesopor. Mater.* **128**, 62–70 (2010).
14. Guo, X. M. *et al.* Incorporation of luminescent lanthanide complex inside the channels of organically modified mesoporous silica via template-ion exchange method. *New J. Chem.* **29**, 1351–1358 (2005).
15. Peng, C. Y. *et al.* Synthesis, characterization, and luminescence properties of the ternary europium complex covalently bonded to mesoporous SBA-15. *J. Phys. Chem. B* **109**, 15278–15287 (2005).
16. Li, S. W. *et al.* Improved photoluminescence properties of ternary terbium complexes in mesoporous molecule sieves. *J. Phys. Chem. B* **110**, 23164–23169 (2006).
17. Kong, L. L., Yan, B. & Li, Y. Hybrid materials of SBA-15 functionalized by Tb<sup>3+</sup> complexes of modified acetylacetonate: covalently bonded assembly and photoluminescence. *J. Alloy. Comp.* **481**, 549–554 (2009).
18. Aisiyah Jenie, S. N. *et al.* Lanthanide luminescence enhancements in porous silicon resonant microcavities. *ACS Appl. Mater. Interface*. **6**, 12012–12021 (2014).
19. Carlos, L. D., Ferreira, R. A. S., Bermudez, V. de Z., Julián-López, B. & Escrivano, P. Progress on lanthanide-based organic-inorganic hybrid phosphors. *Chem. Soc. Rev.* **40**, 536–549 (2011).
20. Han, W. Q., Brutchey, R., Tilley, T. D. & Zettl, A. Activated boron nitride derived from activated carbon. *Nano Lett.* **4**, 173–176 (2004).
21. Vinu, A. *et al.* Synthesis of mesoporous BN and BCN exhibiting large surface areas via templating methods. *Chem. Mater.* **17**, 5887–5890 (2005).
22. Schlienger, S. *et al.* Micro-, mesoporous boron nitride-based materials templated from zeolites. *Chem. Mater.* **24**, 88–96 (2012).
23. Li, J. *et al.* Porous boron nitride with a high surface area: hydrogen storage and water treatment. *Nanotechnology*. **24**, 155603 (2013).
24. Li, J. *et al.* Activated boron nitride as an effective adsorbent for metal ions and organic pollutants. *Sci. Rep.* **3**, 3208 (2013).
25. Weng, Q. H., Wang, X. B., Bando, Y. & Golberg, D. One-step template-free synthesis of highly porous boron nitride microsponges for hydrogen storage. *Adv. Energy Mater.* **4**, 1301525 (2014).
26. Weng, Q., Wang, X. B., Zhi, C. Y., Bando, Y. & Golberg, D. Boron nitride porous microbelts for hydrogen storage. *ACS Nano*. **7**, 1558–1565 (2013).
27. Lei, W. W., Portehault, D., Liu, D., Qin, S. & Chen, Y. Porous boron nitride nanosheets for effective water cleaning. *Nat. Commun.* **4**, 1777 (2013).
28. Lin, J. *et al.* Ultrafine porous boron nitride nanofibers synthesized via a freeze-drying and pyrolysis process and their adsorption properties. *RSC Adv.* **6**, 1253–1259 (2016).
29. Zhi, C. Y. *et al.* Phonon characteristics and cathode luminescence of boron nitride nanotubes. *Appl. Phys. Lett.* **86**, 213110 (2005).
30. Huang, Y. *et al.* Bulk synthesis, growth mechanism and properties of highly pure ultrafine boron nitride nanotubes with diameters of sub-10 nm. *Nanotechnology*. **22**, 145602 (2011).
31. Sabbatini, N., Guardigli, M. & Lehn, J. M. Luminescent lanthanide complexes as photochemical supramolecular devices. *Coord. Chem. Rev.* **123**, 201–228 (1993).
32. Driesen, K., Van Deun, R., Görrler-Walrand, C. & Binnemans, K. Near-infrared luminescence of lanthanide calcein and lanthanide dipicolinate complexes doped into a silica-PEG hybrid material. *Chem. Mater.* **16**, 1531–1535 (2004).
33. Zhang, X. H. *et al.* Blue emitting BCNO phosphors with high quantum yields. *J. Mater. Chem. C* **3**, 3311–3317 (2015).
34. Zhang, X. H. *et al.* Effects of carbon and oxygen impurities on luminescence properties of BNCO phosphor. *J. Am. Ceram. Soc.* **97**, 246 (2014).
35. Liu, Q. *et al.* Synthesis and luminescent properties of Eu(TTA)<sub>3</sub>·3H<sub>2</sub>O nanocrystallines. *Luminescence*. **25**, 307–310 (2010).

## Acknowledgements

This work was supported by the National Natural Science Foundation of China (51372066, 51202055, 51402086, 51572068), the Program for Changjiang Scholars and Innovative Research Team in University (PCSIRT: IRT13060), the Hundred Talents Program of Hebei Province (E2014100011), the Natural Science Foundation of Hebei Province (E2016202122), and the Tianjin Research Program of Application Foundation and Advanced Technology (14JCYBJC42200).

## Author Contributions

J.L. and Y.H. conceived and designed the experiments. J.L., C.F., X.H., W.W., Y.F. and J.L. performed the experiments and analyzed the data. J.L. and Y.H. performed the TEM characterization. J.L., C.F., Z.L., C.T. and Y.H. wrote the manuscript. All authors discussed and commented on the manuscript.

## Additional Information

**Supplementary information** accompanies this paper at <http://www.nature.com/srep>

**Competing financial interests:** The authors declare no competing financial interests.

**How to cite this article:** Lin, J. *et al.* Europium (III) Organic Complexes in Porous Boron Nitride Microfibers: Efficient Hybrid Luminescent Material. *Sci. Rep.* **6**, 34576; doi: 10.1038/srep34576 (2016).



This work is licensed under a Creative Commons Attribution 4.0 International License. The images or other third party material in this article are included in the article's Creative Commons license, unless indicated otherwise in the credit line; if the material is not included under the Creative Commons license, users will need to obtain permission from the license holder to reproduce the material. To view a copy of this license, visit <http://creativecommons.org/licenses/by/4.0/>

© The Author(s) 2016